Composite Structures 327 (2024) 117669

Contents lists available at ScienceDirect

Composite Structures

journal homepage: www.elsevier.com/locate/compstruct

Numerical simulations and experimental results of the deployment of thin-walled bistable composite booms

Daniele Tortorici [a], Marco Sabatini [b], Susanna Laurenzi [a,*]

[a] Department of Astronautical Electrical and Energy Engineering, Sapienza University of Rome, Via Salaria 851-881, 00138 Rome, Italy
[b] School of Aerospace Engineering, Sapienza University of Rome, Via Salaria 851-881, 00138 Rome, Italy

ARTICLE INFO

Keywords:
Thin-walled composites
FEM analysis
Composite structures

ABSTRACT

For advanced space missions, meeting the concurrent requirements of increasing payload size while minimizing spacecraft volume can be achieved through the utilization of deployable structures. In a previous study, we conducted a characterization of a thin/walled boom in terms of its interaction between attitude and elastic dynamics when fully deployed. In this current work, we have developed a numerical model to analyze the critical phase of the deployment process. We compared the model's predictions with theoretical expectations and experimental data, and found a strong agreement between them. Additionally, we investigated the effects of bistability on the deployment process by conducting experiments on both a bistable and a monostable boom. Lastly, we performed deployment tests on a free-floating platform, which emulates a small satellite, to quantitatively measure the attitude perturbations caused by the rapid deployment of the boom.

1. Introduction

Since the advent of space science, the reduction of spacecraft size has been one of the most challenging objectives. This endeavor aims to utilize smaller launchers, which require less volume for the fairing, or to launch multiple satellites in a single launcher, resulting in cost reduction [1–3]. However, this requirement may conflict with the operational performance of certain components, making the study of deployable structures a necessity [4]. Deployable structures possess the ability to exist in either a compact or a deployed configuration. Among these structures, cylindrical booms are commonly used. They find numerous applications, such as passive attitude control systems [5], structural supports for thin-film antennas [6] or solar sails [7,8], and the distancing of sensors from the spacecraft body, as demonstrated by the BepiColombo magnetometer [9]. More recently, booms have been proposed for the design of deployable telescopes [10] and docking systems [11].

Over the years, various technological solutions have been conceived for the realization and deployment of booms [12–18]. Among them, coilable booms are thin-walled open-section structures that can be rolled on the short edge, providing a high packing factor. The use of composite materials allows to meet the requirement of lightweight yet strong boom structures [19]. Due to its space-engineering attractive features, this category is the one selected for this work. By carefully designing the material, it becomes possible to achieve three different types of stable booms: monostable, bistable, and neutrally stable. The type of stability depends on the number of configurations the booms can adopt: one, two, or infinite, respectively [20,21]. Except for the neutrally stable case, automatic deployment of the booms can be accomplished by harnessing the elastic energy accumulated in the boom during the coiling process [20,22]. In these situations, it is essential to incorporate a containment mechanism to prevent any unintended or undesired deployment [23].

Numerous studies have delved into the behavior of thin-walled deployable booms, accompanied by the development of analytical models that elucidate their characteristics. These models encompass aspects such as the existence of a coiled stable state, the energy stored during the folding process, and the laws governing their deployment [20,24–28]. Furthermore, the transition between various configurations stands as a pivotal facet necessitating thorough examination [29]. Typically, booms are manufactured in their stable deployed configuration, which gives rise to challenges during the coiling phase preceding stowage. The assurance of a secure rolling or folding of booms has captivated the attention of numerous researchers, who have conducted both experimental and numerical investigations to assess the feasibility of folding booms safely [16,30–32]. Moreover, the folding behavior has been analyzed from an analytical perspective by Liu et al.[33], who

* Corresponding author.
E-mail address: susanna.laurenzi@uniroma1.it (S. Laurenzi).

https://doi.org/10.1016/j.compstruct.2023.117669
Received 31 July 2023; Received in revised form 6 September 2023; Accepted 26 October 2023
Available online 29 October 2023

devised a model rooted in Archimedes' helix, yielding commendable congruence with experimental and numerical findings.

While efforts have been made to ensure safe coiling or folding, relatively less attention has been dedicated to investigating the deployment phase and this study aims to cover this gap deepening some our previous research [34]. Theoretical models of the deployable phase have been developed [20,24–27], but they often rely on specialized assumptions that may not accurately represent real-world scenarios. However, it is essential to emphasize that the deployment phase is of utmost importance, as any failure during this stage can significantly impact the success of the boom's mission [9,35].

The significance of this concern has garnered the attention of several authors. Strauber et al. [36] have observed that, in the absence of suitable countermeasures, the deployment process can become highly chaotic. Fernandez and Lee [37,38] assert that this issue can be effectively addressed by employing bistable booms, which offer a more controllable self-deployment in comparison to monostable ones. Further insights into this topic have been provided by Murphey et al.[39]. They elucidate the link between the presence of a second stable configuration and a unique kinematic path during the rolling or unrolling of the boom, resulting in predictable and repeatable deployment sequences.

With these considerations in mind, our research focus has been directed towards the investigation of a bistable boom. The primary objective of this study is to conduct a comprehensive analysis of the deployment phase of a thin-walled bistable composite boom, employing a combination of numerical simulations and experimental data. Our overarching aim is to validate the results derived from the numerical model by comparing them with experimental measurements and theoretical predictions, thus showing the possibility of using numerical simulations in the study of deployment. The development of reliable numerical simulations plays a crucial role in cases where theoretical models introduce approximations, and conducting experimental campaigns proves to be both costly and logistically challenging [40]. In this context, the finite element method (FEM) software Abaqus FEA has demonstrated success in simulating thin-walled structures in previous studies [41,42], making it the software of choice for this investigation. In addition to understanding and predicting the dynamics of the deployment phase, the study also focuses on investigating how the deployment process can interact with the satellite that hosts the boom. To achieve this, the researchers conducted deployment tests on a free-floating platform that simulates a real small satellite. The platform is equipped with side panels that mimic solar panels or antennas, and accelerometers are used to measure data during the deployment tests. Moreover, the study incorporates a monostable ultrathin boom from a previous work [43] to evaluate and compare the influence of bi-stability on the deployment behavior. This allows for a direct comparison between the deployment characteristics of monostable and bistable booms, providing valuable insights into their respective performance and suitability for specific satellite applications.

The work is organized as follows: section 2 describes the materials employed and the manufacturing process of the thin-walled bistable boom. Then, in section 3 the characterization of the laminate which constitutes the boom is described. Section 4 presents the theoretical model for the deployment adopted in this study, while section 5 and 6 treat respectively the experimental deployment tests and the numerical model developed to describe them, with relevant results discussed in section 7. The free-floating platform tests are treated in section 8 before section 9 concludes the work, highlighting the most valuable results of the study.

2. Materials and fabrication

The bistable boom was manufactured using two layers of the 1 k bidirectional carbon fiber fabric with a fiber orientation angle of ± 45° and an epoxy resin called PRIME20LV, which is a two-component epoxy resin. The selection of a slow hardener was important to allow sufficient processing time during the construction. To achieve the deployed form of the boom, the fabric was molded onto a rigid cylinder coated with Teflon. The Teflon coating facilitated the demolding process, ensuring that the boom could be removed from the mold without damage. The composite was manufactured following the vacuum bagging technique (Fig. 1).

Fig. 2 shows both the coiled and deployed configurations of the manufactured bistable boom, providing a visual representation of how the boom appears in its stored and fully extended forms. The geometric properties of the boom, as shown in Fig. 3, are as follows: a length (l) of 1 m, a radius (R) of 38 mm, and a subtended angle (β) of 241° in the deployed configuration. Conversely, in the coiled configuration, it is characterized by a radius (r^*) of 45 mm. The thickness is measured to be 0.30 mm.

The fiber volume fraction of thin-walled bi-stable composite boom has been calculated using the following equation:

$$v_f = \frac{nA_W}{\rho_f t} \tag{1}$$

where $n = 2$ is the number of layers, A_W and ρ_f are the areal weight and density of the carbon fiber fabric respectively, which are given from the datasheet (94 g/m^2 and 1.76 g/cm^3), t is the measured thickness. After performing the calculation, the resulting fiber volume fraction is found to be 0.36.

3. Determination of the mechanical properties of laminate

The mechanical properties of the boom laminate were determined through a multiscale numerical analysis. This process involved starting with data on the matrix and fabric and then calculating the properties of a single layer of the composite material, followed by analyzing the two-layer laminate. The Digimat software was utilized for this purpose. To model the single layer of the composite material, the mechanical properties of both the matrix and carbon fibers (as listed in Table 1) were used as input. Additionally, the textile parameters of the fabric (listed in Table 2) were incorporated to construct the representative volume element (RVE).

Fig. 4 depicts the finite element model of the RVE of the fabric. A voxel mesh of $3{\cdot}10^5$ brick elements was used, according to the guidelines in the software. The number of finite elements in the model was determined through a convergence analysis, which aimed to calculate the axial Young modulus of the composite as shown in Fig. 5. The convergence analysis identified a threshold where further refinement of the mesh does not significantly improve the accuracy of the solution. This step ensured that the model was adequately refined to provide reliable results for the mechanical properties of the boom laminate.

After completing the analysis and using the classic laminate theory to determine the properties of the two-layer composite with fiber orientation angles ±45° that make up the boom, the material properties are represented in the form of a constitutive matrix. This matrix is evaluated

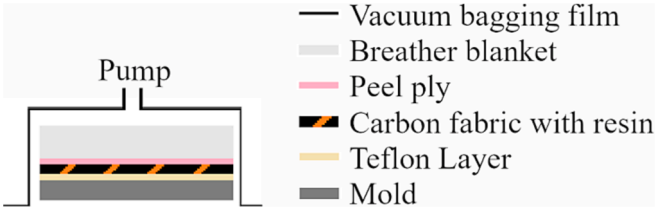

Fig. 1. The scheme illustrates the boom manufacturing process utilizing the vacuum bagging technique. the procedure involves the placement of fabric onto the mold, which is then impregnated with resin. to achieve a smooth surface, a peel ply layer and a breather blanket are applied. the curing process occurs under vacuum conditions, effectively eliminating air bubbles and enhancing the material's density and strength.

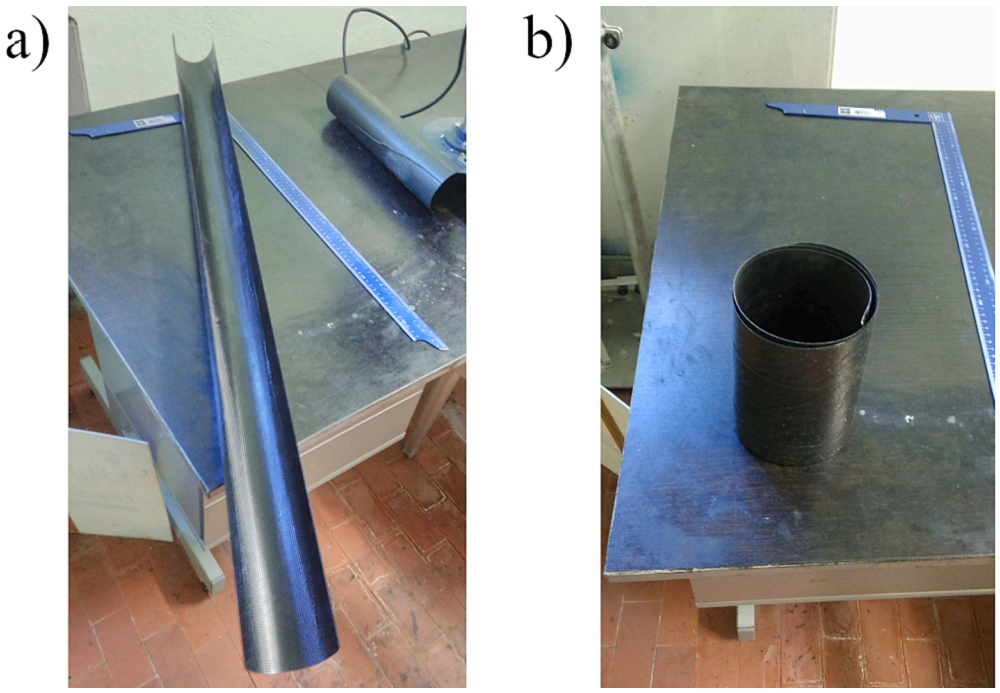

Fig. 2. Thin-walled bistable composite boom in deployed (a) and coiled (b) configurations.

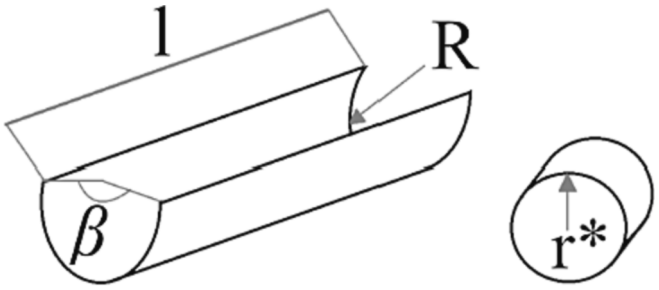

Fig. 3. Geometric parameters of the deployed and coiled configurations of the boom.

Table 1
Microscopic properties of the phases constituting the laminate.

Material	Properties	Value
Resin	density	1.14 g/cm^3
	Young modulus	3.5 GPa
	Poisson ratio	0.35
Fibers	density	1.76 g/cm^3
	axial Young modulus	233 GPa
	transversal Young modulus	23.1 GPa
	in plane Poisson ratio	0.2
	transverse Poisson ratio	0.29
	shear modulus	8.96 GPa

Table 2
Fabric properties.

Yarn linear density	66 tex/km
Fiber diameter	7 μm
Height of yarn cross section	0.06 mm
Width of yarn cross section	1.42 mm
Warp/weft yarn count	7 yarns/cm
Yarn spacing ratio	0.187
Yarn crimp	0.5

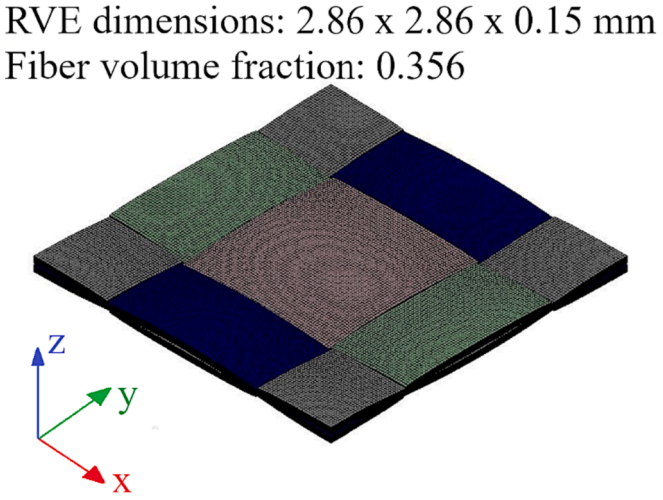

Fig. 4. RVE of fabric. The matrix phase is not visualized for illustration purposes.

through its 3x3 submatrices, denoted as A, B, and D (equation (2).

The constitutive matrix, along with the density (ρ) that has been calculated to be 1.34 g/cm^3, will now be utilized to define the material for the FEM ~~finite element method (FEM)~~ analysis.

$$ABD[+45^\circ/-45^\circ] = \begin{bmatrix} A & B \\ B & D \end{bmatrix} = \begin{bmatrix} 7658 & 6214 & 0 & 0 & 0 & 0 \\ 6214 & 7658 & 0 & 0 & 0 & 0 \\ 0 & 0 & 5949 & 0 & 0 & 0 \\ 0 & 0 & 0 & 57.4 & 46.6 & 0 \\ 0 & 0 & 0 & 46.6 & 57.4 & 0 \\ 0 & 0 & 0 & 0 & 0 & 44.6 \end{bmatrix} \quad (2)$$

The units for A_{ij} are N/mm and Nmm for D_{ij}. B results to be a null matrix, this means there is no coupling between bending and extension.

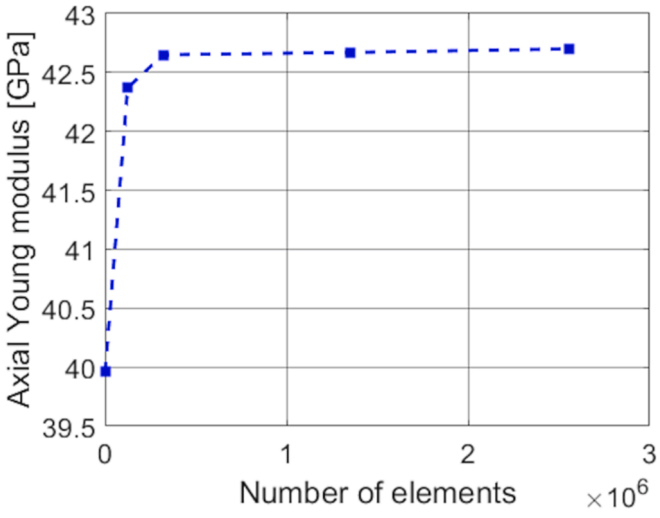

Fig. 5. Convergence analysis for RVE discretization.

4. Theoretical model of the deployment phase

The deployment process of the boom occurs from the coiled configuration to the deployed configuration. The deployed configuration represents the shape given to the boom during its manufacturing, and in this state, no elastic energy is stored in the material. However, in the coiled configuration, the boom holds a positive amount of stored energy due to the work required to roll it into that state. A theoretical model capable of describing both the equilibrium configurations (coiled and deployed) and the deployment process was elaborated in the work by Iqbal and Pellegrino [20] and Guest and Pellegrino [25]. While other models exist in the literature, such as the beam model or the shell model developed by Galletly and Guest [26,27], this particular model stands out for its compactness and ability to analytically capture all the key effects and main features of the deployment problem [25]. The model describes the bending potential energy, possessed by the boom per unit length l, in terms of the curvatures ~~K_x~~ k_x and ~~K_y~~ k_y, considering a generic configuration as defined in Fig. 6. The ability to encompass both equilibrium configurations and deployment dynamics makes this theoretical model a powerful tool in studying and engineering the boom's performance in real-world applications.

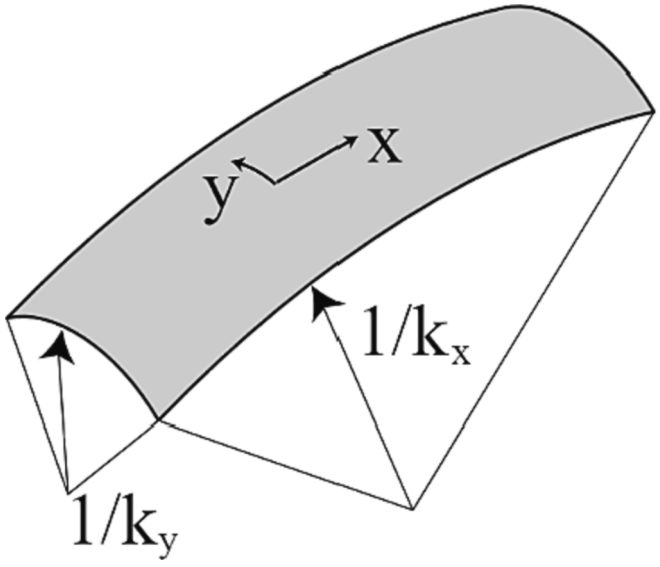

Fig. 6. Generic configuration of the boom where ~~K_x~~ k_x and ~~K_y~~ k_y are the curvatures [25].

According to this model, the elastic bending energy U_b can be written as:

$$U_b = \frac{\beta R}{2}\left[D_{11}{k_x}^2 + 2D_{12}k_x\left(k_y - \frac{1}{R}\right) + D_{22}\left(k_y - \frac{1}{R}\right)^2\right] \tag{3}$$

Neglecting the mixed curvature configuration, the analysis of the function U_b (k_x, k_y,) is conducted by assuming $k_x = 0$ and $k_y = 0$ alternately. This approach helps in identifying two equilibrium configurations (Fig. 3). When $k_x = 0$, the result is as follows:

$$U_b = \frac{\beta R}{2}D_{22}\left(k_y - \frac{1}{R}\right)^2 \tag{4}$$

$$\frac{\partial U_b}{\partial k_y} = \beta R D_{22}(k_y - \frac{1}{R}) \tag{5}$$

$$\frac{\partial^2 U_b}{\partial k_y^2} = \beta R D_{22} \tag{6}$$

The curvature at which $\frac{\partial U_b}{\partial k_y} = 0$ is $k_y = 1/R$. In this case, k_x is assumed to be 0, making it the deployed configuration. This equilibrium configuration is stable because the second derivative has a positive sign, which is a result of being the product of three positive terms. In this deployed configuration, the value of U_b is 0.

For $k_y = 0$, it results:

$$U_b = \frac{\beta R}{2}(D_{11}k_x^2 - \frac{2D_{12}k_x}{R} - \frac{D_{22}}{R^2}) \tag{7}$$

$$\frac{\partial U_b}{\partial k_x} = \beta R(D_{11}k_x - \frac{D_{12}}{R}) \tag{8}$$

$$\frac{\partial^2 U_b}{\partial k_x^2} = \beta R D_{11} \tag{9}$$

The curvature at which $\frac{\partial U_b}{\partial k_x} = 0$ is given by $k_x = \frac{D_{12}}{D_{11}}\frac{1}{R}$, assuming $k_y = 0$. This configuration is referred to as the coiled one. It is a stable equilibrium since the second derivative has a positive sign, which arises from being the product of three positive terms. In this coiled configuration, the potential energy U_b can be calculated as follows:

$$U_b = \frac{\beta R}{2}(\frac{D_{11}}{r} - \frac{2D_{12}}{rR} - \frac{D_{22}}{R^2}) \tag{10}$$

It is important to note that the boom can be coiled at any radius r, but the only radius that will result in a stable configuration is the one that satisfies the condition

$$r^* = \frac{D_{11}}{D_{12}}R \tag{11}$$

Using our design values, we determined that $r^* = 46.8mm$. However, during the production of the boom, we measured r^* to be 45 mm. This resulted in a percentage discrepancy of about 4 %, which can be attributed to the hand lay-up fabrication process.

As mentioned earlier, there are other methods developed to describe the bistable behavior of a boom. One such method is the beam model [26], which considers the twist of the boom. However, in this particular study, we neglected the twist since it becomes significant when D_{13} and D_{23} are different from zero, which is not the case in our study.

Another model, proposed by the same authors, is the shell model [27], which focuses on the importance of the subtended angle (β) on the coiled stable equilibrium configuration, especially when β has a small value. However, once again, in our study, the subtended angle ~~(β)~~ does not have a small value, making this model's considerations irrelevant for our specific case.

Regarding the deployment process, we can quantify the bending

energy ~~(U_b)~~ as a function of the coiled length (x) using linear interpolation between the two extremal values found for the fully coiled and fully deployed configurations. The expression for U_b is given by Equation (12):

$$U_b = \frac{\beta R}{2}\left(\frac{D_{11}}{r} - \frac{2D_{12}}{rR} - \frac{D_{22}}{R^2}\right)x \tag{12}$$

The ejection force, which is the force responsible for the deployment, can be determined by taking the derivative of the bending energy with respect to x [44,45]. The expression for the ejection force (F) is provided in Equation (13):

$$F = \frac{\partial U_b}{\partial x} = \frac{D_{11}\beta}{2R}\left(\frac{D_{22}}{D_{11}} - \frac{2R}{r}\frac{D_{12}}{D_{11}} + \frac{R^2}{r^2}\right) \tag{13}$$

These equations help us analyze the deployment process and understand the forces involved in achieving stable configurations.

The kinetic energy owned from the boom during the deployment is quantified as a function of the undeployed length x:

$$\epsilon = \frac{1}{2}m(l-x)v^2 + \frac{1}{2}m(l-x)r^2\omega^2 \tag{14}$$

Here, two components are evident: the first one is related to the ejection velocity (v), and the second is related to the angular speed (ω); where m represents the mass per unit length. Since $\omega = v/r$, it leads to the following expression:

$$\epsilon = m(l-x)v^2 \tag{15}$$

This equation quantifies the kinetic energy (ϵ) per unit length of the boom during deployment. The value of l corresponds to the initial length of the boom when the deployment starts, and x represents the undeployed length. The deployment speed ~~(v)~~ can be determined by equating the kinetic energy ~~(ϵ)~~ to the work done by the net ejection force $F(1\text{-}\mu)$, as described in reference [44]:

$$v = \sqrt{\frac{F(1-\mu)x}{m(l-x)}} \tag{16}$$

μ is a friction coefficient that has been empirically determined to have an adequate value of 0.6 [46]. With this information, the deployment time (t) can be evaluated using the equation provided earlier:

$$t = \frac{x}{v} \tag{17}$$

With this model, we are able to predict the deployment time as the boom proceeds through the ratio x/l as the independent variable. Analyzing the function $F(r)$ given in equation (1 3~~8~~), we can observe that the coiling radius at which the minimum value for the ejection force occurs is $r = r^*$. This is an expected outcome, and it is anticipated that experimental results will validate this finding. Additionally, to account for the aerodynamic effects, we considered the subtraction of the aerodynamic force from the releasing force in the model. The aerodynamic force $F_{aero} = \frac{1}{2}\rho C_D v^2 A_F$, where A_F is the surface area facing the air given by $A_F = 2\beta R r$, and C_D is the drag coefficient with a value of 1.17, as per reference [44]. Consequently, in equation (16), we used $F - F_{aero}$ rather then F. By including the aerodynamic force, the model provides a more comprehensive representation of the deployment dynamics, considering the impact of air resistance on the ejection force during the deployment process.

5. Wall-fixed experiments of deployment phase

The experimental setup, as shown in Fig. 7, involved connecting the boom to a wall and testing its deployment at several values of the coiling radius (r). The purpose of these experiments was to empirically measure the influence of the coiling radius on the deployment time. By varying the coiling radius, the researchers sought to understand how this parameter affects the time it takes for the boom to deploy fully. In the experimental setup, the boom is rolled into a non-equilibrium state using a containing mechanism. This mechanism prevents the boom from being stored in its equilibrium-coiled configuration (Fig. 2b1d) because self-deployment would not occur in such a case. To enable automatic deployment, an unrolled end of the boom is left, which allows the boom to open once the containing mechanism is released. By adjusting the tightness of the containing mechanism, different coiling radii can be tested, and the mechanism is manually released to trigger the deployment. In addition to testing the bistable boom's deployment, a monostable boom is also tested for comparison. The monostable boom was produced for a previous work [43]. This comparison is carried out to examine how bistability influences the deployment dynamics in comparison to the monostable counterpart. The monostable boom is made by one ply of a 2 × 2 twill fabric made of carbon fiber 3 K-TR30 and R450 epoxy. It is characterized in the deployed configuration by a radius R of 30 mm and a subtended angle of β of 340°.

Fig. 7. Setup for the wall fixed tests.

By conducting these experiments with both the bistable and monostable booms, we can gain insights into the impact of bistability on the deployment process. Furthermore, it is important to note that direct comparisons of deployment times may carry less significance, as the two prototypes exhibit distinct materials and geometries. Understanding how the coiling radius and bistability affect deployment time and dynamics can be crucial for optimizing boom designs for specific applications, such as space missions or engineering structures.

The connection of the boom to the wall was achieved by securing it to a C-shape support and then gluing the support to the wall. This method ensured stability and allowed for consistent positioning during the deployment experiments. To capture the deployment process, a camera with a frame rate of 30 frames per second (FPS) was used. Filming the deployments at this frame rate allowed for detailed analysis and observation of the boom's motion as it unfolded. By recording the deployments using the camera, researchers were able to analyze the entire process frame by frame. This analysis would include measuring the time it took for the boom to fully deploy at various coiling radii ~~(r)~~ and comparing the deployment dynamics between the bistable boom and the monostable boom.

6. Finite element analysis

Numerical analysis was conducted using the Abaqus FEA software. Specifically, the Explicit Dynamic tool was employed due to its efficiency in handling dynamic processes with geometry changes and its ability to accurately capture the non-linear behavior of the problem [16,47]. As previously mentioned, self-deployment is facilitated by the energy stored during the folding phase. To simulate this process, we

defined the boom in its deployed configuration and then applied loads and rotations to gradually return it to the pre-deployment state. It was crucial to apply these loads smoothly, and to ensure accurate results, dissipation energy steps were incorporated before initiating the deployment simulation.

By using the Explicit Dynamic tool in Abaqus, we could effectively model the dynamic behavior of the boom during the deployment process, considering the complex geometric changes and non-linear effects. This numerical approach allowed us to study and understand the self-deployment mechanism and the energy transfer that enables the boom to unfold spontaneously.

The material properties of the boom were characterized using the density and the ABD matrix, as prior research has demonstrated the effectiveness of this approach in overcoming the limitations of the classic laminate theory, particularly concerning the bending properties of ultrathin composites [48–50]. By adopting the density and ABD matrix, we could accurately model and analyze the behavior of the boom during deployment. Similar to Section 3, we conducted a convergence analysis to determine the optimal mesh for the numerical simulation. In this process, we performed a frequency analysis, which proves to be highly efficient even when a large number of elements are used in the simulation. The results of this analysis are presented in Fig. 8. According to the frequency analysis, we found that a mesh with approximately $4{\cdot}10^4$ elements achieves an error of approximately 1 %. This level of error is considered acceptable for achieving reliable and precise results in the subsequent numerical simulations and analyses. By using this well-converged mesh, we can ensure accurate representation of the boom's complex behavior and dynamics during the simulation, enabling a comprehensive understanding of its self-deployment mechanism.

To replicate the setup of the experimental deployment tests, we modeled a portion of the wall where the boom is fixed, along with the necessary components and constraints. To simulate the flattening process, we applied a pressure load on the internal surface of the boom and defined a fictitious horizontal plate. For both the wall and the plate, all degrees of freedom were fixed to ensure accurate simulation. The assembly of the parts with the highlighted constraints is depicted in Fig. 9a.

To enable the interaction between surfaces, we used the General Contact setting. This allowed for surface-surface interaction between the boom and the wall/plate during the analysis.

The analysis was divided into six different and successive steps. These steps include the flattening and coiling phases, which gradually return the boom to its pre-deployment configuration. After these steps, the constraints are removed, and the actual deployment process occurs.

In Table 3, the relevant loads and boundary conditions used in the analysis are presented, helping to accurately simulate the experimental deployment setup. By meticulously defining the constraints and interactions between surfaces, the numerical analysis closely replicates the actual experimental conditions, providing valuable insights into the boom's behavior during self-deployment.

The simulation time plays a crucial role in accurately capturing the deployment dynamics of the boom. It, in combination with the applied loads and rotations, guides the evolution of the process. Therefore, finding the appropriate combination of these parameters is essential to obtain a realistic simulation of the deployment process. To correctly apply the loads and rotations, the "smooth step" command is used [48]. This command defines an application curve corresponding to a fifth-order polynomial with zero first and second derivatives at both the beginning and end of the specified time interval. This ensures a smooth and gradual application of loads and rotations during the simulation. The boundary conditions described earlier and shown in Fig. 9a remain active throughout all simulation steps, in addition to those specified in Table 3. These conditions are crucial for maintaining the integrity and stability of the boom during the analysis. Furthermore, three sets of nodes are defined to change the boom's configuration. The set "node A" comprises the nodes along the free short edge of the boom, while the set "node B" includes the nodes along both long edges of the boom (Fig. 9b). Additionally, a cutting plane is defined at a distance of 100 mm from the constrained edge of the boom. This cutting plane is used to divide the part of the boom that will not be rolled from the rest, and it is represented as set C (Fig. 9c).

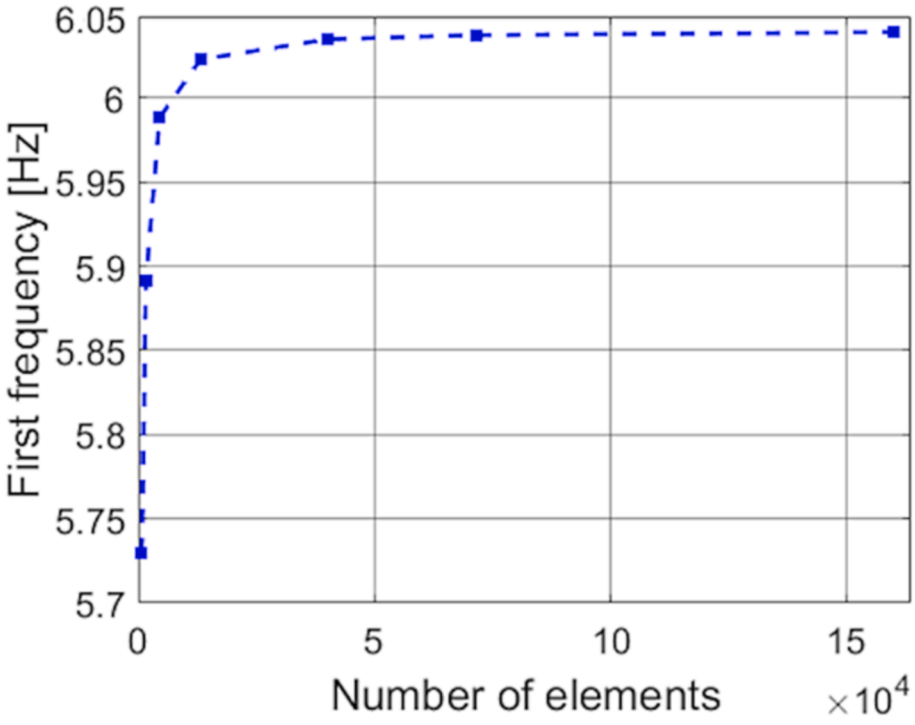

Fig. 8. Convergence analysis for boom discretization.

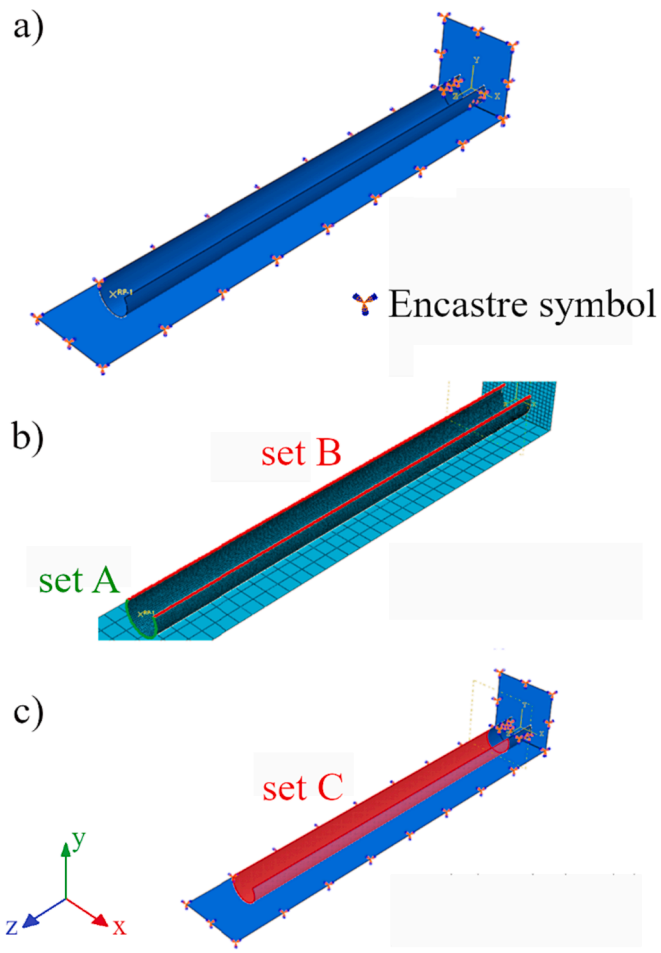

Fig. 9. A) assembly of the boom along with the supports to model the coiling/deployment sequence, with emphasis on the fixed boundary condition; b) nodes designated as set a + B, which are instrumental in altering the boom's configuration; c) Set C, delineating the region critical for achieving the pre-deployment configuration.

Table 3
Constraints and loads applied to the boom for the dynamic analysis.

Step	Phase	Applied loads	Loads' application regions	Applied BC
1	Flattening	Internal pressure Gravity	Boom internal surface All parts	– -
2	Coiling	Internal pressure Gravity	Boom internal surface All parts	Rotation of Set A around x axis (please refer to Fig. 9)
3	Energy dissipation	Internal pressure Gravity	Boom internal surface All parts	Encastre of Set A and B translational and rotational degrees of freedom
4	Adjustment	Gravity	All parts	–
5	Energy dissipation	Gravity	All parts	Encastre of set C translational and rotational degrees of freedom
6	Deployment	Gravity	All parts	–

7. Results and discussion

In the following sections, we present the results obtained from the experimental findings, numerical simulations, and the adopted theoretical model described in Section 3. We will begin by discussing the experimental data and observations regarding the deployment process.

7.1. Experimental results

Fig. 10 and Fig. 11 illustrate the deployment sequence of the bistable and monostable booms, respectively. In the case of the bistable boom, it undergoes a gradual unrolling process, progressively reacquiring its cylindrical shape. The deployment is characterized by a smooth and controlled motion, maintaining stability throughout the unfolding process.

Conversely, the monostable boom demonstrates a different deployment behavior. It tends to rapidly reacquire its cylindrical shape, resulting in an irregular unrolling with a sudden "elbow-like" opening. The deployment of the monostable boom lacks the same level of smoothness and stability observed in the bistable boom, leading to a less predictable and less controlled unfolding.

Furthermore, while the bistable boom deploys in a repetitive and predictable manner, the monostable boom assumes different and irregular configurations in each experiment. This observation underscores the clear advantage of bistable booms over monostable ones, even when not fully coiled, due to their more manageable and consistent deployment behavior. The consistent and predictable behavior of the bistable boom during deployment further highlights its superiority over the monostable boom design.

According to the theoretical model presented in Section 43, the longest deployment time for the bistable boom is expected to occur in correspondence with the coiled stable configuration, which was predicted to happen at a coiling radius of $r = 45$ mm. The experimental data from Table 4 shows that the coiling radius that actually results in the greatest deployment time is measured at $r = 44.9$ mm. The deviation of 0.1 mm between the theoretically predicted value and the experimental result is relatively small and may be within the margin of error for the experimental measurements.

7.2. FEM results

The results obtained from the numerical simulations are presented in terms of the configurations assumed by the boom at various steps, as defined in Table 3. The simulation sequence begins with the boom being flattened by applying an internal pressure, causing it to spread out in a planar configuration. Subsequently, the boom is coiled by rotating the free short edge, which induces it to wrap around a central axis. Fig. 12 displays the most illustrative frames obtained from the simulation, capturing key moments during the folding process. These frames provide

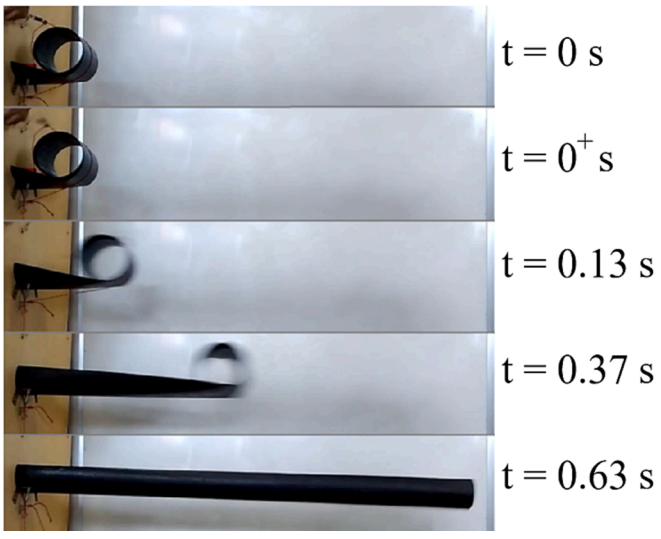

Fig. 10. Deployment sequence of the bistable boom.

Fig. 11. Deployment sequence of the monostable boom.

a visual representation of how the boom undergoes the transition from a flattened state to a coiled configuration and eventually to the fully coiled state.

In Fig. 13, a detailed view of the coiled boom when it reaches the pre-deployment configuration is depicted. During this step, the inner curls of the boom have the opportunity to slide until the outer coiling radius is attained. This movement enables the boom to dissipate any residual excess of accumulated energy, a phenomenon also observed during the experimental tests. Once the pre-deployment configuration is reached, the boom is ready to deploy.

In Fig. 14, the deployment sequence of the boom is illustrated, starting from the moment when all the constraints on the boom are removed. The time count begins at the initiation of the deployment step. The sequence starts from the pre-deployment position, and as the deployment proceeds, the boom progressively unrolls. During the unrolling process, the portion of the boom that is being released starts to reacquire its cylindrical shape. This behavior is a key characteristic of the bistable boom design, where the inherent stability ensures a controlled and predictable deployment.

7.3. Results comparison

In Fig. 15, the relative deployed length of the boom is plotted against time, and the results from both numerical simulations and theoretical predictions are compared with the experimental data. The deployment process initiates at approximately $x/l \cong 0.2$, accounting for the initial dimensions of the coiled configuration. Remarkably, the experimental data closely mirrors the predictions of the theoretical model, represented by the solid line. This congruence serves as a validation of the model's accuracy in forecasting the boom's deployment behavior. The disparities between experimental data and theoretical predictions do not exceed 9 %. This minor variation can primarily be attributed to the resolution of the measurements, as the frames are extrapolated from vide os recorded at a frame rate of 30 FPS. The uncertainty in time measurements is quantified as ± 0.0167 s, resulting in an associated position uncertainty of ± 2.64 cm, based on the average speed. In summary, the experimental data closely aligns with the theoretical model, affirming the reliability and efficacy of the model in predicting the deployment dynamics of the bistable boom. Furthermore, the numerical model also faithfully replicates the phenomenon of the boom's deployment.The predicted deployment time obtained from the numerical model is 0.660 s for a coiling radius of $r = 45$ mm. On the other hand, the experimental measured time is $t = 0.630$ s, resulting in a small discrepancy of 4.5 % between the two values. This indicates that the numerical model is capable of accurately predicting the deployment time, and its results closely match the experimental data.

The good agreement between the numerical model and experimental data is not only limited to the overall deployment time but also holds true for intermediate positions during the deployment process, as demonstrated in Fig. 15. This consistency can also be observed when comparing the deployment sequences in Figs. 9 and 14.

Overall, this comprehensive comparison of the numerical simulations with experimental data and theoretical predictions demonstrates the success of the numerical model in providing reliable insights into the boom's deployment process and behavior, confirming its effectiveness for practical applications in the field of self-deploying structures.

Indeed, bistability plays a crucial role in achieving more regular and controlled deployments compared to the monostable case. The bistable design allows the boom to have two stable configurations, one coiled and one fully deployed. This characteristic ensures that the boom remains stable during both the coiling and deployment phases, leading to smoother and more predictable unfolding behavior. It was observed that the minimum ejection force, which is crucial for initiating the deployment, is achieved at a coiling radius that corresponds to the value of the rolled stable configuration. This means that when the boom is stowed at this specific coiling radius, the deployment requires the least amount of force to initiate, resulting in a more efficient and controlled self-deployment process. However, if the boom is stowed in either a smaller or larger coiling radius, it will lead to faster deployments. This is because deviating from the optimal coiling radius increases the stored energy in the boom, which results in a more rapid release of energy during deployment, causing the boom to unroll faster.

While faster deployments may be desirable in some applications, they can also lead to higher forces and perturbations during deployment, affecting the stability and performance of the overall system. Therefore, finding the right balance between deployment speed and stability is essential in designing self-deploying structures.

8. Free-floating platform experiments

In the final phase of the study, the bistable boom was connected to a free-floating platform, as shown in Fig. 16. The primary objective of this experiment was to evaluate the planar forces and solicitations induced by the deployment phenomenon. To achieve this, the platform was equipped with an accelerometer, and data were acquired during a series of seven deployment tests.

The accelerometer data played a crucial role in identifying the different phases of the deployment process. Acceleration peaks in the data served as markers, demarcating the beginning and ending of the deployment sequence. These peaks allowed researchers to precisely determine when the self-deployment was initiated and when it was completed.

During the experiments, the self-deployment of the bistable boom was triggered by an electric actuator, which unlocked the containing mechanism. This mechanism was responsible for holding the boom in its coiled configuration until it was ready to deploy. Once released, the boom underwent the self-deployment process as observed in previous tests.

Table 4
Measured deployment time for various radius.

r [mm]	37.1	37.9	38.2	38.5	39.2	43.4	44.0	44.9	45.5	47.0	47.5	47.8
t [s]	0.53	0.53	0.57	0.53	0.53	0.57	0.60	0.63	0.60	0.57	0.60	0.50

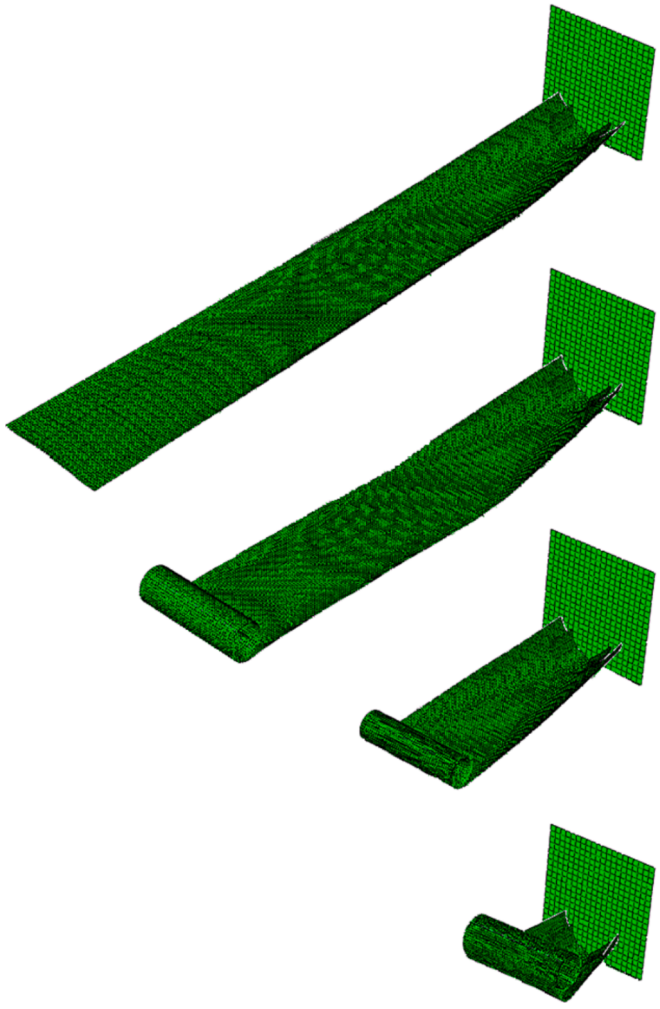

Fig. 12. Flattening and coiling sequence obtained from FEM analysis.

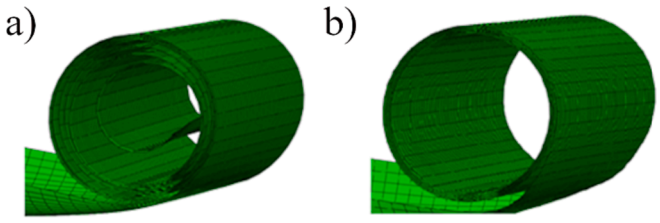

Fig. 13. Pre-deployment configuration of the boom.

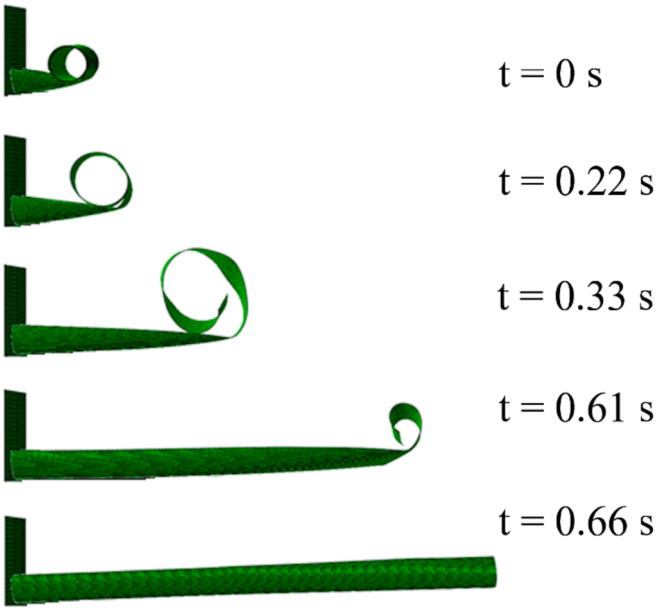

Fig. 14. Deployment sequence of the boom.

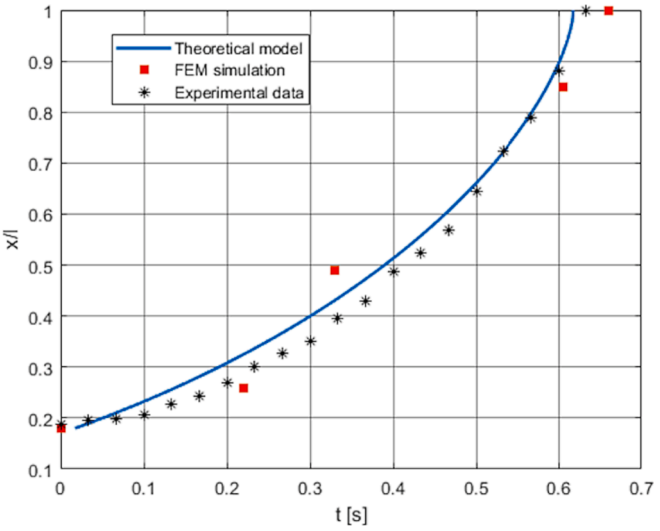

Fig. 15. Deployment evolution comparison.

In all the tests conducted, a consistent and similar behavior was observed during the deployment of the bistable boom. The relationship between deployment time and coiling radius exhibited the same trend as seen in previous experiments. Fig. 17 illustrates the accelerometer measurements during a deployment test where the boom had a coiling radius of 45.1 mm. The data was acquired over a duration of 25 s, with a sampling frequency of 70 Hz. The deployment command was initiated at $t = 5$ s.

The results in Fig. 17 show that the deployment process begins at $t = 5.53$ s and concludes at $t = 6.16$ s, with a total deployment time of 0.63 s. This deployment time value closely aligns with the findings from the fixed wall test for a similar coiling radius. However, it is noteworthy that a different method was employed to measure the deployment time in this case. Instead of relying on vide o acquisition, the beginning and ending of the deployment were determined based on the peaks observed in the axial acceleration data recorded by the accelerometer. The similarity in deployment behavior and the close agreement in deployment times across various tests further validate the reliability and consistency of the bistable boom's performance. The use of accelerometer measurements for detecting the deployment phases provides an alternative and complementary approach to vide o analysis, proving to be effective in accurately identifying the start and end of the deployment process. Overall, the experimental findings from the accelerometer measurements reaffirm the predictability and stability of the bistable boom's self-deployment, making it a viable and promising option for deployment systems in practical engineering applications.

The analysis of the measured accelerations revealed some interesting observations during the deployment of the bistable boom connected to the free-floating platform. One notable finding was the presence of a larger peak in the accelerations at the end of the deployment. This peak was attributed to the impulsive stop of the boom's motion as it reached its fully deployed configuration. The sudden deceleration at the end of the deployment process resulted in a higher acceleration amplitude.

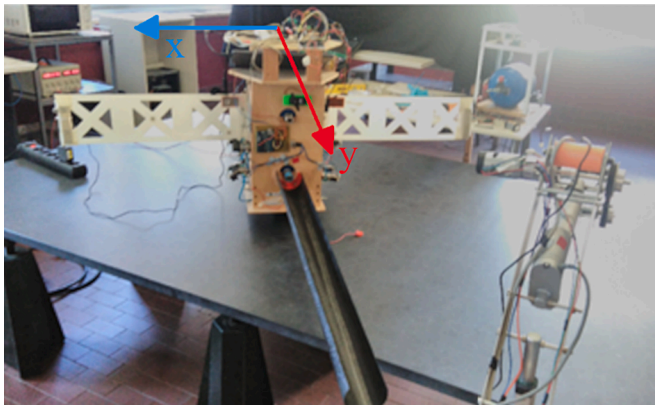

Fig. 16. Image illustrates the boom on the free-floating platform, with the reference frame of the accelerometers. in this frame: the x-axis runs parallel to the panels' axis; the y-axis is aligned with the deployed boom, orthogonal to the x-axis; the z-axis represents the vertical direction.

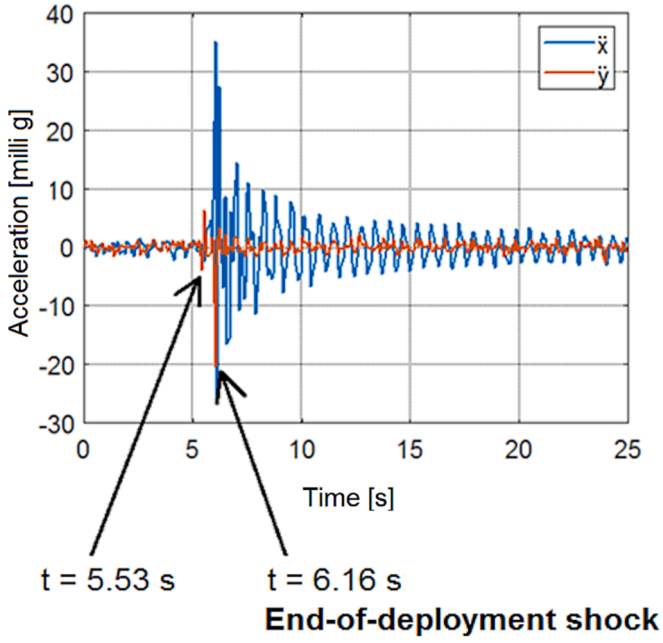

Fig. 17. Measured planar acceleration during deployment phase.

The difference in acceleration amplitudes between the x and y components was attributed to the positioning of the accelerometer. The accelerometer's orientation made the measurement in the x- direction more sensitive, leading to a higher amplitude in that direction compared to the y-direction.

Additionally, two unexpected phenomena were observed during the experiments. Firstly, the platform experienced a rotary motion around its z-axis. This unexpected rotation was attributed to asymmetries and imprecisions in the connection of the boom to the platform, which generated a torque during the deployment process. Secondly, the experiment showed the excitation of the platform's side panels. These panels, being elastic structures, started to oscillate as a consequence of the dynamic excitation during the deployment of the boom. This observation highlights the importance of considering the dynamic interactions between the boom and other components of the system, as they can influence the overall stability and behavior during deployment. The observed phenomena demonstrate the complexity and interconnected nature of the deployment process in real-life applications. They emphasize the significance of conducting comprehensive experimental tests to capture the dynamic behavior and solicitations experienced by the entire system during deployment. The observations from the fixed-wall tests can be extended to the boom constrained only to the floating platform. The end of deployment shock, characterized by a larger peak in accelerations, remains proportional to the deployment time. In other words, when the boom undergoes a faster deployment, it experiences a larger shock at the end of the deployment process. This finding highlights the importance of carefully controlling the deployment process to achieve a balance between deployment speed and the associated shock amplitude. While faster deployments may be desirable in some scenarios, they can lead to higher forces and vibrations that may affect the stability and performance of the entire system.

9. Conclusion

In this study, the deployment phase of a thin-walled bistable composite boom was thoroughly investigated through both numerical simulations and experimental tests. The results obtained from the numerical and theoretical analysis closely matched the experimental data for the bistable boom fixed to a wall. The key aspects analyzed were the deployment times and the dynamic behavior during the deployment process. A maximum difference of 4.5 % in terms of deployment time was observed between the numerical model and the experimental data. This slight deviation could be attributed to variations between the theoretical properties of the laminate used in the boom's construction and the actual properties of the prototype, likely caused by minor inefficiencies in the manufacturing process. Despite this discrepancy, the numerical model still aligned well with the theoretical predictions for the considered geometry and boom type. The advantage of using numerical finite element method predictions is that they provide more general solutions, as they can consider the real geometry of the boom without imposing any specific limitations. In contrast, analytical models may be limited by certain assumptions about the geometry, making FEM simulations a more versatile approach.

Additionally, the deployment of the produced bistable boom was compared to a monostable boom from a previous work. The results revealed that the bistable boom exhibited a more manageable and controlled behavior during deployment, further confirming the superiority of bistable designs for self-deploying structures. Finally, the deployment of the bistable boom was observed while connected to a free-floating platform, simulating the deployment phase on a real small satellite. The results demonstrated that a rapid deployment phase induced linear acceleration and attitude perturbations of the platform, leading to vibrations of other flexible appendages like solar panels. The most significant perturbations occurred towards the end of the deployment process. Acceleration peaks of 35 milli g in the x-direction and 20 milli g in the y-direction were recorded as soon as the boom reached its fully deployed state. These peaks were notably larger than the ones detected at the beginning of the deployment, which measured at 3 milli g and 5 milli g in the x and y directions, respectively. Furthermore, these peak amplitudes exhibited an inverse relationship with deployment time. Additionally, it was observed that asymmetries could induce a rotational motion of the platform. This underscores the importance of considering the effects of boom deployment when designing satellite deployment systems.

In conclusion, this comprehensive investigation into the deployment phase of the bistable boom provided valuable insights into its behavior and performance. The excellent agreement between numerical, theoretical, and experimental results confirmed the accuracy of the models and validated the advantages of using bistable booms in various applications, particularly those requiring precise and controlled self-deployment.

CRediT authorship contribution statement

Daniele Tortorici: Investigation, Formal analysis, Validation,

Writing – original draft. **Marco Sabatini:** Investigation, Formal analysis, Methodology, Writing – review & editing. **Susanna Laurenzi:** Methodology, Conceptualization, Formal analysis, Supervision, Funding acquisition, Writing – review & editing.

Declaration of Competing Interest

The authors declare that they have no known competing financial interests or personal relationships that could have appeared to influence the work reported in this paper.

Data availability

Data will be made available on request.

Acknowledgment

The work was financed by the European Union - NextGenerationEU (National Sustainable Mobil-ity Center CN00000023, Italian Ministry of University and Research Decree n. 1033 - 17/06/2022, Spoke 11 - Innovative Materials & Lightweighting). The opinions expressed are those of the authors only and should not be considered as representative of the European Union or the European Commission's official position. Neither the European Union nor the European Commission can be held responsible for them.

References

[1] Gibbons D, Holemans W. Packaging multiple small satellites on a single launch vehicle. 3rd Utah State University Conference on Small Satellites. 1989.
[2] Lal B, de la Rosa BE, Behrens JR, Corbin BA, Green E, Picard AJ, et al. Global trends in small satellites. IDA Science and Technology Policy Institute Alexandria 2017.
[3] Peloni A, Barbera D, Laurenzi S, Circi C. Dynamic and structural performances of a new sailcraft concept for interplanetary missions. Scientific World Journal 2015; 2015.
[4] Puig L, Barton A, Rando N. A review on large deployable structures for astrophysics missions. Acta Astronaut 2010;67:12–26.
[5] Hooker W, Leliakov I, Lyons M, Margulies G. Reaction-boom attitude control systems. J Spacecr Rocket 1970;7:1337–43.
[6] Tan LT, Pellegrino S. Thin-shell deployable reflectors with collapsible stiffeners Part 1: approach. AIAA J 2006;44:2515–23.
[7] Block J, Straubel M, Wiedemann M. Ultralight deployable booms for solar sails and other large gossamer structures in space. Acta Astronaut 2011;68:984–92.
[8] Seefeldt P, Grundmann JT, Hillebrandt M, Zander M. Performance analysis and mission applications of a new solar sail concept based on crossed booms with tip-deployed membranes. Adv Space Res 2021;67:2736–45.
[9] Heyner D, Auster HU, Fornaçon KH, Carr C, Richter I, Mieth JZD, et al. The BepiColombo Planetary Magnetometer MPO-MAG: What Can We Learn from the Hermean Magnetic Field? Space Sci Rev 2021;217:52.
[10] De Zanet G, Viquerat A, Aglietti G. Predicted thermal response of a deployable high-strain composite telescope in low-Earth orbit. Acta Astronaut 2023;205: 127–43.
[11] Takao Y, Mori O, Ji K. Analysis and design of a spacecraft docking system using a deployable boom. Acta Astronaut 2021;179:172–85.
[12] Schenk M, Viquerat A, Seffen K, Guest S. Review of Inflatable Booms for Deployable Space Structures: Packing and Rigidization. AIAA. J Spacecr Rocket 2014;51.
[13] Katsumata N, Natori MC, Yamakawa H. Analysis of dynamic behaviour of inflatable booms in zigzag and modified zigzag folding patterns. Acta Astronaut 2014;93:45–54.
[14] Li N, Peng H, Li F. Instantaneous optimal control of inflatable folded structures. Acta Astronaut 2022;195:52–67.
[15] Mobrem M, Adams D. Deployment Analysis of Lenticular Jointed Antennas Onboard the Mars Express Spacecraft. J Spacecr Rocket 2009;46:394–402.
[16] Stabile A, Laurenzi S. Coiling dynamic analysis of thin-walled composite deployable boom. Compos Struct 2014;113:429–36.
[17] Leipold M, Daton-Lovett A. Highly compact deployable and retrievable boom. In: 57th International Astronautical Congress; 2006. p. C2. 03..
[18] Zhang Z, Zhou H, Ma J, Xiong L, Ren S, Sun M, et al. Space deployable bistable composite structures with C-cross section based on machine learning and multi-objective optimization. Compos Struct 2022;297:115983.
[19] Murphey TW, Francis W, Davis B, Mejia-Ariza JM. High strain composites. 2nd AIAA spacecraft structures conference2015. p. 0942.
[20] Iqbal K, Pellegrino S. Bi-stable composite shells. In: 41st Structures, Structural Dynamics, and Materials Conference and Exhibit; 2000. p. 1385.
[21] Schultz MR, Hulse MJ, Keller PN, Turse D. Neutrally stable behavior in fiber-reinforced composite tape springs. Compos A Appl Sci Manuf 2008;39:1012–7.
[22] Seffen K, Pellegrino S. Deployment dynamics of tape springs. Proceedings of the Royal Society of London Series A: Mathematical, Physical and Engineering Sciences. 1999;455:1003-48.
[23] Jeon S, Murphey T. Design and analysis of a meter-class CubeSat boom with a motor-less deployment by bi-stable tape springs. 52nd AIAA/ASME/ASCE/AHS/ ASC Structures, Structural Dynamics and Materials Conference 19th AIAA/ASME/ AHS Adaptive Structures Conference 13t2011. p. 1731.
[24] Liu T-W, Bai J-B. Fantuzzi N. Folding behavior of the thin-walled lenticular deployable composite boom: Analytical analysis and many-objective optimization. Mechanics of Advanced Materials and Structures; 2022. p. 1–19.
[25] Guest S, Pellegrino S. Analytical models for bistable cylindrical shells. Proceedings of The Royal Society A: Mathematical, Physical and Engineering Sciences 2006; 462:839–54.
[26] Galletly DA, Guest SD. Bistable composite slit tubes. I. A beam model. Int J Solids Struct 2004;41:4517–33.
[27] Galletly DA, Guest SD. Bistable composite slit tubes. II. A shell model. Int J Solids Struct 2004;41:4503–16.
[28] Tianwei L, Jiangbo B, Fantuzzi N. Analytical model for predicting folding stable state of bistable deployable composite boom. Chin J Aeronaut 2023.
[29] Leclerc C, Pedivellano A, Pellegrino S. Stress concentration and material failure during coiling of ultra-thin TRAC booms. In: 2018 AIAA Spacecraft Structures Conference; 2018. p. 0690.
[30] Bai J-B, Chen D, Xiong J-J, Shenoi RA. Folding analysis for thin-walled deployable composite boom. Acta Astronaut 2019;159:622–36.
[31] Liu T-W, Bai J-B, Xi H-T, Fantuzzi N, Bu G-Y, Shi Y. Experimental and numerical investigation on folding stable state of bistable deployable composite boom. Compos Struct 2023;320:117178.
[32] Liu T-W, Bai J-B, Fantuzzi N, Xi H-T, Xu H, Li S-L, et al. Folding behavior of thin-walled tubular deployable composite boom for space applications: Experiments and numerical simulation. Acta Astronaut 2023;209:159–71.
[33] Liu T-W, Bai J-B, Fantuzzi N. Analytical models for predicting folding behaviour of thin-walled tubular deployable composite boom for space applications. Acta Astronaut 2023;208:167–78.
[34] Sabatini M, Tortorici D, Laurenzi S. Numerical simulations and experimental tests for the deployment of a thin-walled bistable composite boom. Proceedings of the International Astronautical Congress, IAC2020.
[35] Rivera A. Study of Spacecraft Deployables Failures. Space Systems Anomalies and Failures (SCAF) Workshop 20222021.
[36] Straubel M, Block J, Sinapius M, Hühne C. Deployable composite booms for various gossamer space structures. 52nd AIAA/ASME/ASCE/AHS/ASC Structures, Structural Dynamics and Materials Conference 19th AIAA/ASME/AHS Adaptive Structures Conference 13t2011. p. 2023.
[37] Fernandez JM, Lee AJ. Bistable collapsible tubular mast booms. International Conference on Advanced Lightweight Structures and Reflector Antennas. 2018.
[38] Lee AJ, Fernandez JM. Inducing bistability in collapsible tubular mast booms with thin-ply composite shells. Compos Struct 2019;225:111166.
[39] Murphey T, Jeon S, Biskner A, Sanford G. Deployable booms and antennas using bi-stable tape-springs. 24th Annual AIAA/USU Conference on Small Satellites. 2010.
[40] Różyło P. Experimental-numerical test of open section composite columns stability subjected to axial compression. Archives of Materials Science and Engineering 2017;84:58–64.
[41] Różyło P, Łukasik D. Numerical analysis of the critical state of thin-walled structure with z-profile cross section. Advances in Science Technology Research Journal 2017;11.
[42] Debski H, Samborski S, Rozylo P, Wysmulski P. Stability and load-carrying capacity of thin-walled FRP composite Z-profiles under eccentric compression. Materials 2020;13:2956.
[43] Laurenzi S, Rufo D, Sabatini M, Gasbarri P, Palmerini GB. Characterization of deployable ultrathin composite boom for microsatellites excited by attitude maneuvers. Compos Struct 2019;220:502–9.
[44] Brinkmeyer A, Pellegrino S, Weaver PM. Effects of long-term stowage on the deployment of bistable tape springs. J Appl Mech 2016;83.
[45] Kajihara S, Yokozeki T, Aoki T. Dimension effects on the stowability and self-deployment behavior of CFRP bistable open-section semi-cylindrical beam. Compos Struct 2023;307:116628.
[46] Rimrott F. STEM self-extension velocities(Theoretical derivation of self-extension velocities of storable tubular extendible member/STEM/). Canadian Aeronautics Space Journal 1967;13:1–7.
[47] Smith M. ABAQUS/standard user's manual. version 2009;6:9.
[48] Barbera D, Laurenzi S. Nonlinear buckling and folding analysis of a storable tubular ultrathin boom for nanosatellites. Compos Struct 2015;132:226–38.
[49] Mallikarachchi C, Pellegrino S. Quasi-Static Folding and Deployment of Ultrathin Composite Tape-Spring Hinges. J Spacecr Rocket 2011;48.
[50] Mallikarachchi C. Thin-walled composite deployable booms with tape-spring hinges. University of Cambridge; 2011.